Development of a riboswitch-based platform for live cell imaging of RNAs in mammalian cells

Esther Braselmann[1,3], Aleksandra J. Wierzba[2,#], Jacob T. Polaski[1,#], Mikołaj Chromiński[2], Dilara Batan[1,3], Dorota Gryko[2], Robert T. Batey[1], Amy E. Palmer[1,3,]*

[1] Department of Chemistry and Biochemistry, University of Colorado, Boulder, CO, USA, 80303

[2] Institute of Organic Chemistry, Polish Academy of Sciences, Kasprzaka 44/52, 01-224 Warsaw, Poland

[3] BioFrontiers Institute, University of Colorado, Boulder, CO, 80303

[#] These authors contributed equally to this work.

*To whom correspondence should be addressed: amy.palmer@colorado.edu

Graphical abstract

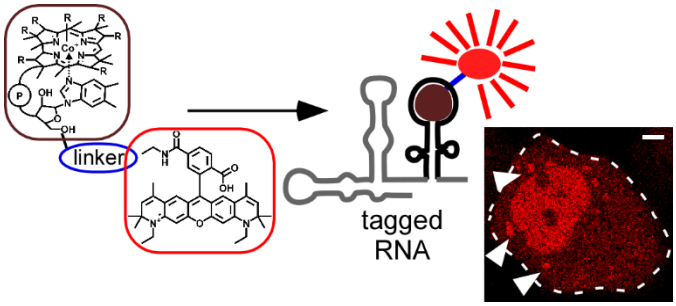

Abstract

RNAs directly regulate a vast array of cellular processes, emphasizing the need for robust approaches to fluorescently tag and track RNAs in living cells. Here, we develop an RNA imaging platform using the Cobalamin (Cbl) riboswitch as an RNA aptamer and a series of probes containing Cbl as a fluorescent quencher linked to a range of fluorophores. We demonstrate fluorescence turn-on upon RNA binding and proof of concept for tracking both mRNA and small U RNA in live cells.

Main text

The complex spatiotemporal dynamics of messenger RNAs (mRNAs) and non-coding RNAs (ncRNAs) affect virtually all aspects of cellular function. These RNAs associate with a large group of RNA binding proteins that dynamically modulate RNA localization, processing and function[1,2]. Such interactions govern mRNA processing, export from the nucleus, and assembly into translationally competent messages, as well as association into large macromolecular granules that are not translationally active, including P-bodies and stress granules (SGs)[3–6]. Similarly, uridine-rich small nuclear RNAs (U snRNAs, the RNA components of the spliceosome)[7] dynamically associate with protein components to comprise the functional spliceosomal complex in the nucleus[8]. During different stresses including bacterial infection, the U snRNAs along with the splicing machinery can be transiently sequestered in cytosolic foci

called U-bodies[7]. Given the intricate connection between RNA localization, dynamics and function, there has been a strong push to develop tools for visualization of RNA in live cells to elucidate mechanisms underlying the mRNA and ncRNA life cycle.

While there is a broad spectrum of tools to fluorescently tag proteins in live cells, far fewer approaches for live cell imaging of RNA exist. The most common system uses a series of tandem hairpins that bind an RNA-binding protein (MS2 or PP7 coat protein) coupled to a fluorescent protein (FP)[9–11]. This system has been used successfully to interrogate mRNA dynamics over time at the single molecule level[9,10]. However, one limitation of this system is that 12-24 copies of the aptamer are required to enhance fluorescence contrast, and the large size of the tag can perturb localization, dynamics and processing[12] of the RNA. An alternative approach involves attaching an aptamer to the RNA that directly binds a small molecular fluorogenic dye[13–16]. Recent years have seen the application of Spinach[17], Broccoli[18], and Mango[19] aptamers to label and track RNAs in live mammalian cells. However, all these aptamers evolved *in vitro* contain a G-quadruplex[20], which has been shown to complicate RNA folding and ligand selectivity in mammalian cells[21–23]. While these tools demonstrate the power and potential of RNA imaging to reveal spatiotemporal dynamics of RNA function, a strong need for robust and complementary approaches for fluorescently tagging and visualizing RNA in live mammalian cells with small molecular probes remains.

Here, we propose an orthogonal approach for fluorescent tagging of RNA in live cells using a bacterial riboswitch as the RNA aptamer and a series of small molecular probes that increase their fluorescence intensity. We took advantage of the robust folding of bacterial riboswitches in different genetic contexts in cells[24,25], while exploiting specific binding of the riboswitch RNA aptamer to its natural ligand, the cofactor cobalamin (Cbl)[26,27]. Cbl functions as an efficient fluorescence quencher when covalently coupled to a synthetic fluorophore[28–30]. We postulated that binding of Cbl to an RNA aptamer could sterically separate the Cbl quencher and covalently coupled fluorophore resulting in fluorescence turn on from a Cbl-fluorophore

probe (Fig. 1a), as demonstrated in similar fluorophore-quencher systems for RNA labelling[15,16]. Structural information of Cbl bound to the aptamer revealed that the Cbl 5'-hydroxyl group is accessible even in the RNA-bound state[26] (Fig. 1b), leading us to choose this position for conjugation with fluorophores via copper catalyzed alkyne-azide cycloaddition reaction[31,32] to explore different conformational and photochemical properties of the probe (Fig. 1c).

To assess how properties of fluorophores affect quenching, a series of probes with different fluorophores conjugated to Cbl via a 6-carbon chain (C6) was synthesized (Supplementary Results, Supplementary Fig. 1). The fluorescence of each probe was measured and compared to that of the free fluorophore (Fig. 1d, Supplementary Fig. 2). Cbl-C6-FAM and Cbl-C6-ATTO 488 retained only 0.5% and 2.5% fluorescence respectively, indicating that quenching, defined as reduction of the fluorescence signal, was most efficient for probes with fluorophores in the green wavelength regime (λ_{em} ~520 nm). In contrast, probes with emission in the far-red range (λ_{em} ~660 nm) retained around 25% fluorescence (22% for Cbl-C6-ATTO 633 and 27% fluorescence for Cbl-Cy5), corresponding to weaker quenching (Fig. 1d). Cbl-C6-ATTO 590 emits in the red range (λ_{em} ~624 nm) and resulted in moderate quenching (5.4% residual fluorescence). Together, the results revealed a correlation between quenching efficiency and the excitation/emission wavelengths of the fluorophore, where quenching was the least efficient in the far-red and most efficient in the green wavelength range.

We systematically assessed how the length of the chemical linker affects quenching and found that increasing the linker length reduces quenching efficiency (Fig. 1d), consistent with similar observations in the literature[28]. Addition of a C6 linker (~3.5 Å, Supplementary Table 3) between Cbl and ATTO 590 resulted in higher residual fluorescence (5.4% for Cbl-C6-ATTO 590 vs. 3.9% for Cbl-ATTO 590). In line with this trend, increasing the linker length further to five polyethylene glycol (PEG) units (~17.5 Å, Supplementary Table 3) increased the residual fluorescence to 8.7%. Similar trends were observed when changing the linker length for probes

with FAM as the fluorophore (Supplementary Fig. 3), confirming that quenching is most efficient when the fluorophore is close to Cbl via a minimal linker.

We hypothesized that binding of an RNA aptamer to the Cbl moiety of our probes would sterically separate fluorophore and quencher and thereby reduce quenching, resulting in an increase in fluorescence (Fig. 1a). To test this, the fluorescence signal of several probes in the presence and absence of a minimal truncated aptamer (A_T) was compared. We also included a control aptamer that harbors four point mutations to abolish binding to Cbl ($A_{T,MUT}$) (Supplementary Fig. 4). As expected, fluorescence increase was observed for all probes upon binding to A_T (Fig. 2a, b, Supplementary Fig. 5). Importantly, signal was not significantly changed in the presence of the negative control aptamer $A_{T,MUT}$ (Fig. 2a, b), and aptamer A_T did not affect the fluorescence signal of the free fluorophore (Supplementary Fig. 6). We further characterized Cbl-5xPEG-ATTO590 and the aptamer A_T biophysically and found that the affinity for Cbl was within the same order of magnitude in the context of the probe (0.29 μM vs. 1.3 μM, Supplementary Fig. 7) and quantum yield measurements were consistent with our plate reader fluorescence assay (Supplementary Fig. 8, Fig. 2b). Together, these observations indicate that fluorescence turn on is specifically induced when the aptamer A_T binds the Cbl portion of the probe.

We predicted that increasing the steric bulk of the aptamer would promote greater separation between Cbl and fluorophore upon binding, leading to a larger fluorescence turn on. To test this hypothesis, we compared fluorescence turn on for Cbl-5xPEG-ATTO 590 in the presence of A_T *vs.* the full-length aptamer A that contains an additional structural element to increase 'bulkiness' (Supplementary Fig. 4). Binding of Cbl-5xPEG-ATTO 590 to A compared to A_T resulted in a modest increase in fluorescence (35% *vs.* 43%, Fig. 2b). To further test the influence of RNA structure, we synthesized two additional aptamers (B and C, Supplementary Fig. 4) derived from other members of the Cbl riboswitch family. Both variants B and C include bulky features that could potentially introduce steric constraints when binding the probe

(Supplementary Fig. 4). Variant B results in a modest improvement in fluorescence turn on compared with variant A_T for most probes tested (Fig. 2a, b). However, variant C did not increase fluorescence turn on of Cbl-5xPEG-ATTO 590 compared to variant A_T (Fig. 2b). Together, while bulky features appended to the aptamer improve fluorescence turn on modestly, we observed no significant increase. Therefore, aptamer A_T was chosen for further characterization and cellular tests.

The observation that spectral properties of the fluorophore impacted the extent of quenching and fluorescence turn on upon aptamer binding suggests that Förster resonance energy transfer (FRET) may contribute to quenching, a hypothesis we evaluated by calculating the Förster radius and estimating the distance between the fluorophore and quencher for each of the probes (Supplementary Tables 2-4). The estimated distance between quencher and fluorophore for probes in the green wavelength range (FAM and ATTO 488 fluorophores) is significantly below the calculated values for R_0, consistent with efficient quenching (< 3% residual fluorescence, Fig. 1d, 2a). In line with this model, even the bulkiest aptamers tested induced fluorescence turn-on that resulted in ~5% or less fluorescence compared with the free fluorophore (Fig. 2a), presumably because the length of the linker does not allow for separation of fluorophore and quencher beyond the R_0 distance. Probes with the ATTO 590 fluorophore have a Förster distance (R_0 = 20 Å) close to the estimated distance between corrin ring and fluorophore (Supplementary Table 4), suggesting that ATTO 590 probes are particularly susceptible to large changes in fluorescence intensity for small distance changes. Together, our theoretical estimates are consistent with a model where FRET contributes to quenching. However, it is noteworthy that conjugates in the far-red wavelength regime (λ_{em} ~660 nm) lack spectral overlap with the Cbl absorbance spectrum (Supplementary Fig. 9), yet moderate fluorescence quenching was still observed, suggesting that non-FRET mechanisms must also contribute to fluorescence quenching.

We tested the riboswitch-based RNA imaging platform in live mammalian cells by visualizing two different RNAs: localization of β-actin mRNA (*ACTB*) to SGs in U2-OS cells (Fig. 3a-d) and sequestration of the non-coding U1 snRNA in U-bodies in HeLa cells (Fig. 3e-g). Two Cbl-fluorophore probes were chosen for live imaging (Cbl-5xPEG-ATTO590 and Cbl-Cy5) because they exhibited the highest fluorescence upon binding the aptamer. Initial iterations of evolved aptamers include a folding scaffold and improved brightness of Spinach 2[33] in mammalian RNAs, but this can lead to unwanted processing. Conversely, the A_T aptamer didn't require the tRNA folding scaffold[34] and exclusion of the scaffold prevented unwanted processing, prompting us to omit this scaffold (Supplementary Fig. 11). Probes localized diffusely in U2-OS cells after bead loading[35–37] (Supplementary Fig. 10a). Treatment of cells with arsenite induces formation of SGs that can be visualized by the GFP-tagged marker protein G3BP1[38–40] (Fig. 3b, 3d). We verified that ACTB mRNA[38,39] tagged with the aptamer A_T localized to G3BP1-positive SGs via fluorescence in situ hybridization (FISH) in fixed cells, similar to endogenous ACTB mRNA (Supplementary Fig. 12). We loaded the Cbl-Cy5 probe in cells transfected with a plasmid to produce the A_T-tagged ACTB mRNA and observed robust accumulation of Cbl-Cy5 fluorescence in SGs upon arsenite treatment when 4 copies of A_T were used (Fig. 3b, c, Supplementary Fig. 13), suggesting that ACTB mRNA recruitment to SGs was visualized via the riboswitch aptamer tag. Importantly, the Cbl-Cy5 fluorescence signal remained diffuse throughout the cytosol in untransfected cells, indicating that Cbl-Cy5 specifically binds to the A_T aptamer (Fig. 3b). Similar results were observed when the probe Cbl-5xPEG-ATTO590 was used (Supplementary Fig. 14). It is important to note that transient transfection efficiency of the tagged mRNA, expression level of mRNA fusions, ACTB mRNA colocalization to SGs (Supplementary Fig. 12) and probe uptake efficiency (Supplementary Fig. 10) are heterogeneous processes, which may explain the broad distribution of Cbl-Cy5 fluorescence increase in SGs (Fig. 3c). To directly confirm that Cbl-Cy5 fluorescence accumulation in SGs is due to the presence of A_T-tagged ACTB mRNA in SGs, we measured

the formation of SGs in live cells and subsequently fixed cells and measured the pattern of A_T aptamer localization by FISH (Supplementary Fig. 15). Together, we confirmed that localization of ACTB mRNA to SGs can be readily visualized in live cells using our riboswitch aptamer system, with the additional benefit of allowing visualization with two orthogonal colors (ATTO590 and Cy5) while keeping the size of the tag below 350 nucleotides (for 4 copies of the A_T aptamer).

The small size of our riboswitch aptamer tag (81 nt for one copy of A_T) allows for tagging of ncRNAs such as snRNA U1 in live cells. Proper processing of U snRNA was found to depend on its length with an overall size limit of 200-300 nucleotides (nt)[41], limiting the size of any U1 fusion tag to ~100 nt. We introduced the aptamer tag near the 5' end of the U1 coding sequence, a position that was previously shown to be compatible with short RNA tags[42]. U snRNAs localize to nuclear Cajal bodies[43], and U1 tagged with our aptamer A_T can also localize to the Cajal body marker protein Coilin in HeLa cells (Supplementary Fig. 16a, b). Treatment of HeLa cells with Thapsigargin induced sequestration of the endogenous U1 snRNA and aptamer-tagged U1 in cytosolic U-bodies that contained the marker proteins DEAD-Box Helicase 20 (DDX20) and survival motor neuron (SMN) (Supplementary Fig. 16c, 17). When loading probes in live HeLa cells, non-specific puncta formation was observed for Cbl-Cy5 (but not for Cbl-5xPEG-ATTO590) (Supplementary Fig. 10b), leading us to choose Cbl-5xPEG-ATTO590 for live U1 snRNA visualization. After Thapsigargin-treatment of cells transiently transfected with the aptamer-tagged U1, 24±10% of cells contained cytosolic puncta resembling U-bodies, whereas such puncta were only observed in 6±3% of untransfected cells (Fig. 3e). These results are in line with reports in the literature, where ~25% of HeLa cells were reported to contain U-bodies upon Thapsigargin-treatment[7]. To confirm that the cytosolic puncta we observed constitute U1 snRNA containing U-bodies, we transiently transfected the GFP-tagged U-body marker protein SMN together with the aptamer-tagged U1 and observed colocalization (Fig. 3f, Supplementary Fig. 18). Together, we conclude that our riboswitch-aptamer based

imaging system allows for live cell visualization of small non-coding RNAs such as the snRNA U1.

The riboswitch-based RNA imaging system presented here includes several unique features that promise broad applicability to visualize diverse RNAs in live cells. By utilizing binding of the aptamer to its native binding partner Cbl, binding specificity between aptamer tag and the probe is ensured. Because the RNA does not bind to the fluorophore directly, our system enables flexibility to include synthetic fluorophores with different spectral properties (Cbl-5xPEG-ATTO590 and Cbl-Cy5). We have assessed the parameter-space of Cbl-fluorophore probes with different organic linkers and fluorophores, and identified quenching and de-quenching trends that may guide future development of this system. The fact that Cbl riboswitches represent a diverse family of sequences may be explored for multiplexing of this system in the future. Lastly, we have demonstrated proof-of principle application of the Cbl-riboswitch based aptamer imaging system in live mammalian cells by visualizing two distinct RNAs, including the small non-coding U1 snRNA.

Acknowledgements

The authors would like to acknowledge financial support from the Human Frontiers Science Project. We acknowledge support from the National Science Centre, SYMFONIA DEC-2014/12/W/ST5/00589 to Dorota Gryko and Aleksandra J. Wierzba and from the National Institutes of Health (5R01 GM073850) to Robert T. Batey. Thanks to Roy Parker, Siddharth Shukla, Joshua Wheeler and Jennifer Garcia for helpful discussions and for providing cell lines, antibodies and plasmids. Thank you to Denise Muhlrad, Jason Lee and Maria Lo for technical expertise and to Jens Eberhard and Jeremiah Gassensmith for helpful discussions. The imaging work was performed at the BioFrontiers Institute Advanced Light Microscopy Core, whose Nikon A1R microscope acquired by the generous support of the NIST-CU Cooperative Agreement award number 70NANB15H226.

Author contributions

EB, JTP, RTB and AEP conceptualized and designed the study. JTP and RTB rationally designed riboswitch variants. EB, JTP, RTB, AJW, DG and AEP designed organic probes. AJW and MC synthesized organic probes. JTP purified riboswitch variants for *in vitro* work. EB performed *in vitro* work and designed and performed cellular work and analyzed data with input from all authors. DB constructed plasmids and assisted with cellular work. EB wrote the manuscript with edits from all authors.

Competing financial interests statement

The authors declare no competing financial interests.

Figures and Figure legends

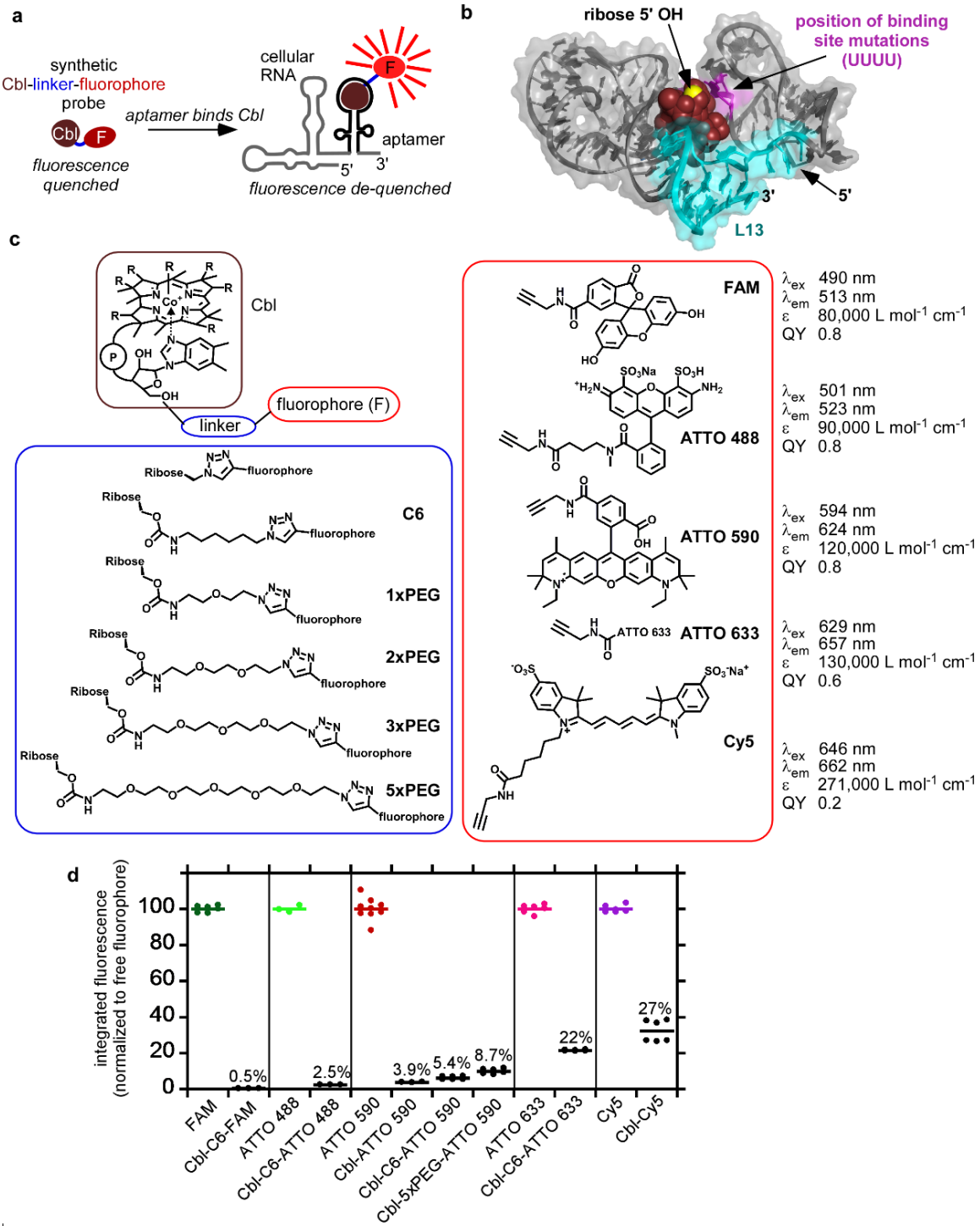

Figure 1: Covalent attachment of different fluorophores to Cobalamin (Cbl) results in fluorescence quenching, allowing for fluorescence turn-on of the probe upon binding to riboswitch RNA. (a) Principle of RNA-induced fluorescence turn-on for Cbl-fluorophore probes.

Cbl (brown circle) acts as a quencher for the covalently attached fluorophore (red oval) due to proximity in space. Upon binding the RNA aptamer, Cbl is sterically separated from the fluorophore, resulting in de-quenching and fluorescence turn on. (b) Structure of the Cbl riboswitch RNA (variant A, see Figure S4) bound to Cbl[26]. Loop P13 (teal) is at the 3'-end of the aptamer. Cbl is shown in red spheres and the 5'- hydroxyl residues at the ribose moiety is shown in yellow. The four bases that were mutated to UUUU to abolish binding to Cbl are shown in magenta. (c) Synthetic Cbl-fluorophore probes used in this study. The organic linker was attached at the 5'- hydroxyl of the ribose and conjugated to alkyne variants of commercially available fluorophores via click chemistry, resulting in the triazole linkage between the linker and fluorophore. Note that the structure of ATTO 633 is proprietary. (d) Comparison of the fluorescence intensity of fluorophore *vs.* Cbl-fluorophore probes. Fluorescence spectra of 5 μM free fluorophores or Cbl-fluorophore probes were collected, the integrated intensity for each free fluorophore was set to 100% and the value for the Cbl-fluorophore probe was normalized relative to that of the corresponding fluorophore. Data are presented as mean for at least n = 3 independent measurements.

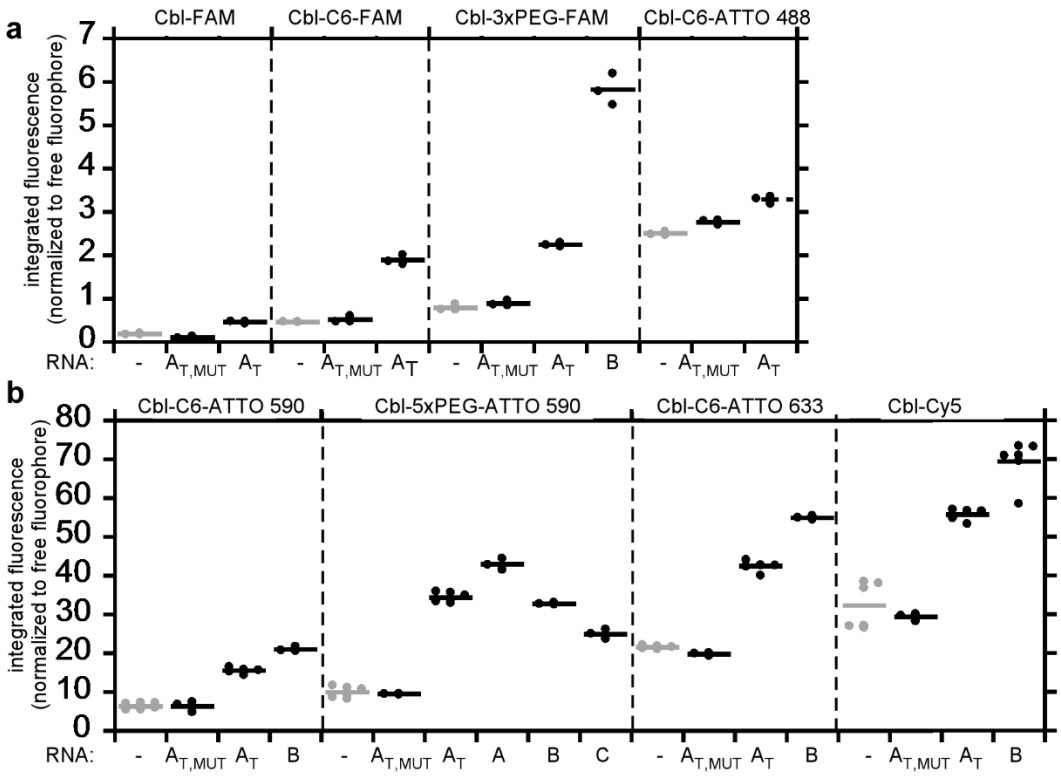

Figure 2: Cbl riboswitch RNAs induce fluorescence turn on in Cbl-fluorophore probes *in vitro*. The fluorescence intensity of Cbl-fluorophore probes in the presence or absence of different RNAs was quantified as in Figure 1d and normalized relative to the intensity of the free fluorophore for 488 nm probes (a) and longer wavelength probes (b). The RNA aptamers A, B and C are variants of Cbl-binding riboswitch sequences, where A_T refers to a truncated version of A with linker region J1/3 and stem-loop P/L13 deleted (see also Figure 1b). The subscript MUT in $A_{T,MUT}$ refers to four point mutations in the Cbl-binding site (see Figure 1b for the position of these residues). Data are presented as mean for n = 3 independent measurements.

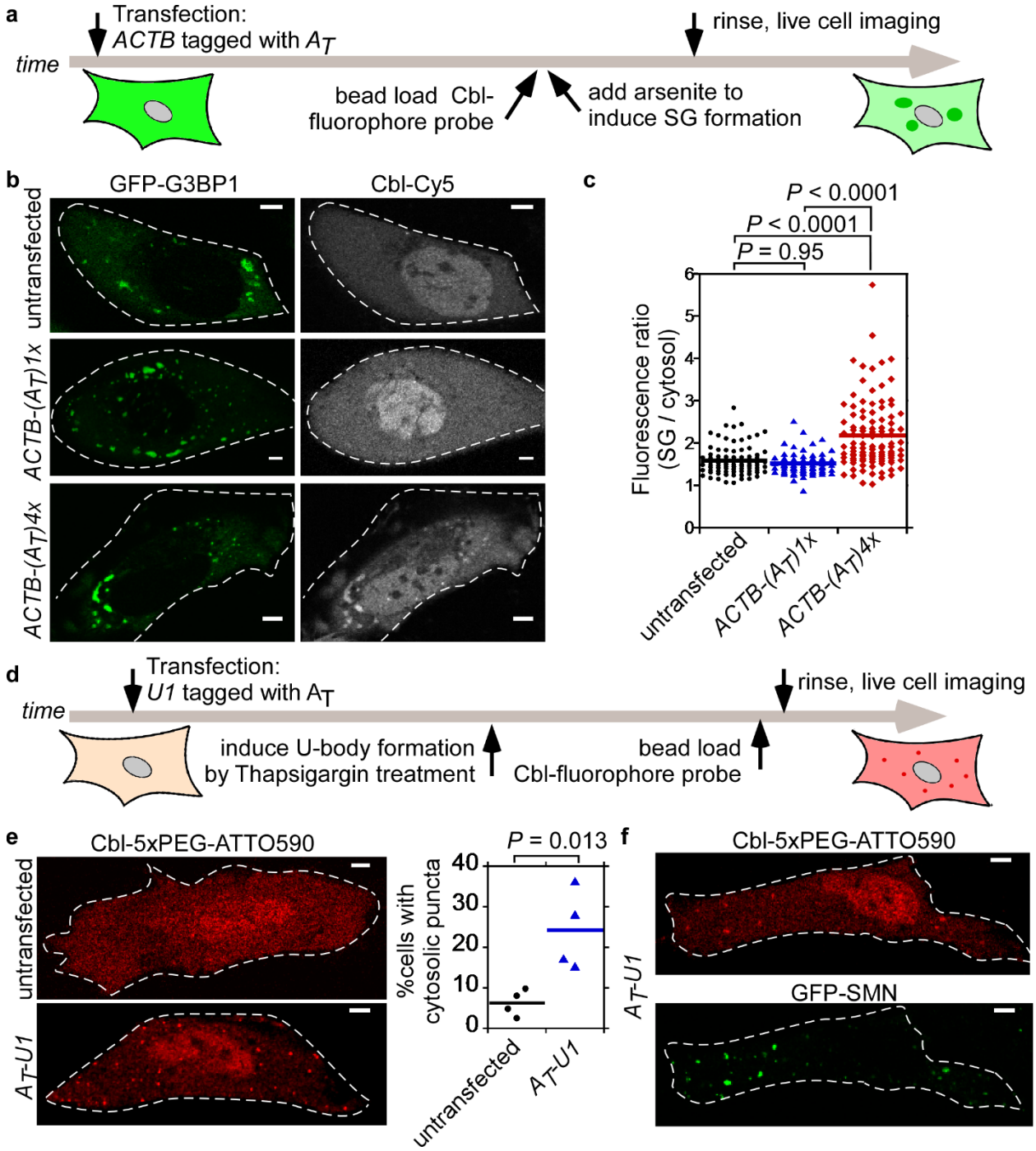

Figure 3: Live cell visualization of mammalian RNAs via binding of the Cbl-fluorophore probes to the genetically encoded RNA tag. (a) Monitoring ACTB mRNA localization to SGs via Cbl-fluorophore probe binding to the A_T tag. (b) The Cbl-Cy5 probe colocalizes with SGs only when ACTB mRNA is tagged with 4 copies of A_T. Cells stably expressing *GFP-G3BP1* were transfected with *ACTB* tagged with 1 or 4 A_T copies. The probe was introduced and SGs were

induced by treatment with 0.5 mM arsenite for 45 min before live microscopy. (c) Cbl-Cy5 accumulation in SGs was quantified via a line trace through each SG and calculating the ratio of signal in the SG over the average cytosol signal (Supplementary Fig. 12). Robust fluorescence increase was only observed for ACTB mRNA tagged with 4 copies of A_T. Untransfected: 4 independent experiments, 37 cells, 63 SGs. *ACTB-(A_T)1x*: 3 independent experiments, 20 cells, 63 SGs. *ACTB-(A_T)4x*: 4 independent experiments, 45 cells, 105 SGs. (d) Monitoring cytosolic U-bodies via *A_T*-tagged U1. After transient transfection of *A_T-U1*, U-bodies were induced by Thapsigargin treatment followed by live cell microscopy. (e) Cbl-5xPEG-ATTO590 localization to cytosolic puncta in Thapsigargin-treated HeLa cells is more likely when *A_T-U1* was transfected (*A_T-U1*: mean from 4 independent experiments / 326 cells; untransfected: mean from 4 independent experiments / 677 cells). (f) Cytosolic puncta in Thapsigargin-treated cells expressing *A_T-U1* co-localize to GFP-SMN U-bodies. 3 independent experiments, 10 cells. Scale bar = 5 μm. (c,e) One way ANOVA (95% confidence limit), post hoc test (Tuskey HSD).

Methods

Synthesis of fluorophore probes

Descriptions of synthesis and characterization of probes can be found in the Supplementary Note. All probes are derivatives of CN-Cbl and structures of all probes used in this study are shown in Supplementary Figure 1. See also Supplementary Table 1 for a summary of photophysical properties.

RNA synthesis and preparation

For all *in vitro* experiments, DNA templates were amplified using recursive PCR and transcribed by T7 RNA polymerase using established methods.[45] Transcription reactions were purified using the appropriate percentage denaturing polyacrylamide gel (8 M urea, 29:1 acrylamide:bisacrylamide) based on RNA length. Transcripts were visualized by UV shadowing, excised from the gel and soaked overnight in 0.5x TE buffer (10 mM Tris-HCl, pH 8.0, 1 mM EDTA) at 4°C. RNAs were buffer exchanged into 0.5x TE and concentrated using centrifugal concentrators (Amicon) with the appropriate molecular weight cutoff. RNA concentration was determined using the absorbance at 260 nm and molar extinction coefficients calculated as the summation of the individual bases. Sequences and secondary structures of all RNAs used in this study are shown in Supplementary Figure 4.

Absorbance measurements and quantum yield determination

Absorbance spectra were collected using a Cary 500 UV-VIS-NIR spectrophotometer and buffer subtracted and measurements were reproducible compared with literature data. The quantum yield (Q) of probes was determined by comparison with the quantum yield of ATTO 590 (Atto tec) and its published quantum yield of 0.80. All experiments were conducted in RNA buffer (100 mM KCl, 10 mM NaCl, 1 mM $MgCl_2$, 50 mM HEPES, pH 8.0). First, absorbance was

determined at the excitation wavelength (Supplementary Table 1) for a dilution series of ATTO 590 and Cbl-5xPEG-ATTO 590 in the presence and absence of aptamer A_T. To ensure saturation of binding, the concentration of A_T was chosen such that the final concentration of A_T was above 5 μM in the most diluted sample. The fluorescence spectrum at the emission range indicated in Table S1 for each sample was then recorded using a PTI-fluorimeter (1 nm steps, 1 s integration time, 2 nm slits for the excitation and 4 nm slits for detector). After subtracting the buffer background signal, the fluorescence signal for each sample was integrated and plotted vs the absorption. The steepness of the resulting linear plot for each dilution series reports on the quantum yield relative to the reference of ATTO 590 (Supplementary Table 2). These measurements were done once for the QY determination, and spectra were comparable with absorbance / fluorescence measurements done for fold fluorescence measurements.

In vitro fluorescence measurements

The concentration of Cbl-fluorophore probes, free fluorophores and free Cbl was determined using extinction coefficients listed in Supplementary Table 1. For the Cbl-fluorophore probes, the extinction coefficient of the fluorophores was used to determine the concentration. The shape of the absorption spectra did not change significantly for the conjugated probes compared with the sum of spectra for free fluorophores and free Cbl (Supplementary Fig. 2). The fluorescence intensity of each probe was measured in the presence or absence of RNA in RNA buffer as technical triplicates in a Tecan Safire-II fluorescence plate. The concentration of the probe was 0.25 μM or 0.5 μM and the RNA concentration was at least 5 μM, significantly above the dissociation constant (K_d) of the RNAs tested[26,27] (see also Supplementary Fig. S7). Samples were incubated for at least 20 min at room temperature in the dark to allow for Cbl-binding of the RNA prior to data collection. The excitation wavelength for each probe is listed in Supplementary Table 1 and the emission

spectrum was collected in 1 nm increments for the range listed in Supplementary Table 1. Each emission spectrum was buffer subtracted, integrated and normalized to the signal of the free fluorophore at the same concentration. Resulting % fluorescence measurements were reproducible for measurements on different days. Representative fluorescence spectra of probes in the presence and absence of RNA are shown in Supplementary Figure 5.

Isothermal titration calorimetry (ITC)

ITC experiments were performed using protocols previously established and described[26,27]. Briefly, the RNA was dialyzed overnight at 4°C into RNA buffer (100 mM KCl, 10 mM NaCl, 1 mM $MgCl_2$, 50 mM HEPES, pH 8.0) using 6-8000 Dalton molecular weight cutoff dialysis tubing (Spectra/Por). The dialysis buffer was used to dissolve Cbl and Cbl-5xPEG-ATTO590, and to dilute RNA to the desired concentration. The concentration of Cbl and Cbl-5xPEG-ATTO 590 was determined using the extinction coefficients listed in Supplementary Table 1. Titrations were performed at 25°C using a MicroCal ITC_{200} microcalorimeter (GE Healthcare) and data were fit using the Origin software suite as previously described[46].

Estimation of theoretical photophysical properties and distances in probes

The overlap integral J(λ) of each fluorophore with Cbl absorbance was calculated from equation (1)[47]:

$$(1) \qquad J(\lambda) = \int_0^\infty F_D(\lambda)\varepsilon_A(\lambda)\lambda^4 d\lambda$$

where F_D is the emission spectrum of the fluorophore normalized to unity and ε_A is the extinction coefficient of the acceptor (Cbl) in M^{-1} cm^{-1} using a MATLAB script (a|e - UV-Vis-IR Spectral Software 1.2, FluorTools, www.fluortools.com). To include the entire fluorescence emission spectrum of each fluorophore (Supplementary Fig. 6), fluorophores were excited 10 nm below the typical (Supplementary Table 1) excitation λ and emission was collected 10 nm above the

excitation λ using a PTI-fluorimeter (1 nm steps, 1 s integration time, 2 nm slits for the excitation and 4 nm slits for detector). Cbl absorbance and fluorophore emission spectra (shown in Supplementary Fig. 9) and were converted in units of M^{-1} cm^{-1} (for absorbance of Cbl) and to unity (for emission of fluorophores) to calculate J(λ). The Förster distance R_0 was calculated from equation (2)[47]

$$R_0 = 0.211(\kappa^2 n^{-4} Q_D J(\lambda))^{\frac{1}{6}} \quad (2)$$

where κ^2 is a factor describing the relative orientations of the transition dipoles and was assumed as $\kappa^2 = 2/3$[47] and the refractive index n was assumed to be 1.4 for aqueous solutions. The quantum yield Q of each donor fluorophore is available from the manufactures of the fluorophores and is listed in Supplementary Table 2.

The maximal distance between quencher and fluorophore in each probe was estimated as the length of the chemical linker (listed in Supplementary Table 3) plus the distance between the 5' hydroxyl moiety of Cbl (where the linker is attached) and the corrin ring in the structure of Cbl[26], assuming that this region of Cbl harbors quenching properties. The distance between 5' hydroxyl moiety and the corrin ring was estimated to be 9 Å from the Cbl crystal structure[26]. This distance was added to each linker lengths, resulting in the distances listed in Supplementary Table 4.

Construction of plasmids for mammalian expression of aptamer variants

Plasmids to produce RNA aptamers fused with RNA of interest in mammalian cells were constructed by standard molecular cloning techniques (see Supplementary Figure 19 for an overview and Supplementary Figure 20 for aptamer sequences). To construct mRNA fusions, the commercially available vector *pmCherry-C1* (Clontech) was used as a starting point, since it harbors the CMV promoter for strong expression in mammalian cells. A *Nhe*I restriction site was introduced immediately following the stop codon by site directed mutagenesis. Different

aptamer sequences were inserted between the stop codon and the polyA site using existing *Kpn*I and *Bam*HI restrictions sites. Inserts encoding for aptamers were purchased as g-blocks or ultramers depending on sequence length with the appropriate restriction site overhangs from IDT. Sequences for aptamers are summarized in Supplementary Figure 4 and the tRNA scaffold previously used in Spinach constructs[17] was used. This strategy resulted in construction of *mCherry-(tRNA-A_T)1x*, *mCherry-(A_T)1x* and *mCherry-(B)1x*. For ACTB mRNA fusions, the coding sequence of *mCherry* was replaced with the *ACTB* coding sequence. The ACTB coding sequence was PCR amplified from a plasmid producing a mNeonGreen-actin fusion (sequence verified to be identical with Homo sapiens beta actin (ACTB), NCBI Reference Sequence NM_001101.3) by standard restriction based cloning using *Nhe*I restriction sites flanking the coding sequence of the *mCherry* gene. As for mCherry fusions, the aptamer tags were purchased as ultramers or gblocks from IDT and added by standard restriction based cloning using existing *Kpn*I and *BamH*I sites. The monomeric tag of the aptamer A_T was introduced by ligating the first g-block into the plasmid with *Kpn*I / *BamH*I restriction sites resulting in *ACTB-(A_T)1x*. Additional copies were introduced sequentially, where the second and third copy was encoded on a g-block with *Kpn*I / *Kpn*I and *BamH*I / *BamH*I restriction sites, respectively, resulting in *ACTB-(A_T)2x* and *ACTB-(A_T)3x*. *ACTB-(A_T)4x* was the result of the third ligation step, where colonies were screened for insertion of more than one copy of A_T.

The existing plasmid p*U1(human)*[48] to produce the A_T-tagged U1 snRNA was modified to add the sequence of the aptamer A_T immediately following the first 11 nucleotides of *U1*, analogous to previous U1 snRNA fusions[42]. Briefly, the parent plasmid was digested with two existing unique restriction sites (*Bgl*II is upstream of the *U1* coding sequence and *Pst*I is in the 3' region of the *U1* coding sequence). An insert that contains the aptamer sequence A_T and the surrounding *U1* coding sequence including both restriction sites was purchased as a g-block from IDT and ligated, resulting in *A_T-U1*. All plasmids were verified by sequencing.

Cell culture and cell lines

U2-OS cells (received from Professor Roy Parker[49]), HeLa cells and 293T cells (both purchased from ATCC) were maintained in Dulbecco's modified eagle medium (DMEM, Gibco) supplemented with 10% fetal bovine serum (FBS; Gibco) at 37°C with 5% CO_2. Cells were not passaged more than 12 times for experiments. To generate a U2-OS cell line that stably produces GFP-G3BP1, the *GFP-G3BP1* coding sequence was PCR amplified from a p*eGFP-C1*-based cloning vector (received from Professor Roy Parker) using *Eco*RI and *Not*I restriction site overhangs. The PCR product was ligated into a Piggybac Dual Promoter plasmid that includes a Puromycin resistance cassette for selection and a CMV promoter for *GFP-G3BP1* expression (System Biosciences, Catalog # PB510B-1), resulting in plasmid p*GFP-G3BP1-Piggybac*. This plasmid was sequence verified. U2-OS cells were chemically transfected with p*GFP-G3BP1-Piggybac* and *Super PiggyBac Transposase* expression vector (System Biosciences, Catalog # PB220PA-1) using the *Trans*IT transfection system according to manufacturer recommendations (Mirus). Selected for genomic integration using was started 3 days after transfection using 1 μg/mL Puromycin and continued for 7-10 days. After selection, U2-OS cells stably expressing *GFP-G3BP1* were FACS enriched for the brightest 30% of GFP-fluorescent cells. After FACS enrichment, cell aliquots were used for up to 10 additional passages.

Bead loading

Cells were seeded in home-made imaging dishes (35 mm diameter) with a ~10 mm center hole covered by cover glass (No. 1.5, VWR). To introduce the probe, the culture media was removed and the Cbl-fluorophore probe (typically 3 μL of a 50 μM stock in PBS) was added directly on the cell in the center of the imaging dish. Microbeads were sprinkled onto the cells[35–

[37] and the dish was tapped on the cell culture surface 7-8 times. Standard culture media supplemented with 0.5 mM sodium arsenite was added immediately

Stress granule (SG) assay

U2-OS cells stably expressing *GFP-G3BP1* were seeded at 0.15x10^6 cells in imaging dishes. One day after seeding, cells were chemically transfected with typically 1 μg plasmid DNA (*ACTB-(A_T)1x*, *ACTB-(A_T)3x* or *ACTB-(A_T)4x*) using the *Trans*IT transfection system following manufacturer recommendations (Mirus). On the next day, cells were bead loaded with the Cbl-fluorophore probe. The media that was added after bead loading contained 0.4 mM sodium arsenite and cells were incubated at 37 °C / 5% CO_2 for 45 min. Cells were rinsed once in PBS and Fluorobrite media (Gibco), supplemented with 0.5 mM sodium arsenite was added for live cell imaging. For correlative live / fixed imaging where cells were first imaged live, before fixation and FISH / immunofluorescence imaging of the same cells, the following modifications were made to the protocol above. Instead of home-made imaging dishes, gridded imaging dishes (MatTek) were used. Dishes were coated with 1 μg/mL fibronectin (Sigma) for 4 hours. Fibronectin was rinsed once with full media before cells were seeded.

U-body assay

HeLa cells were seeded at 0.1 - 0.15 x 10^6 cells per imaging dish. One day after seeding, cells were chemically transfected with 1 μg plasmid DNA (*A_T-U1*) using the *Trans*IT transfection system following manufacturer recommendations (Mirus). For experiments with marker proteins, 0.25 μg of GFP-SMN[50] (a gift from Greg Matera, Addgene plasmid #37057) or was co-transfected. For colocalization experiments with Coilin, 0.5 μg pEGFP-coilin[51] (a gift from Greg Matera, Addgene plasmid #36906) was transfected with our without co-transfection of 0.5 μg plasmid DNA encoding for *A_T-U1*. Imaging or fixation was performed the following

day. For live cell imaging, cells were treated with 10 μM Thapsigargin for 3 hours before bead loading with the Cbl-fluorophore probe and imaged within 1 hour after bead loading. For immunofluorescence or FISH analysis, cells were fixed 3-4 hours after Thapsigargin treatment.

Fluorescence microscopy and image analysis

Fluorescence microscopy on live and fixed cells was performed on a Nikon A1R Laser Scanning Confocal Microscope with a 100x oil objective (1.45 NA, Plan Apo I), a pixel size of 0.25 μm and an integration time of 2.2 μsec unless otherwise noted below. Images were acquired at 16-bit depth with Nikon Elements Software and processed in ImageJ2 using the Fiji plugin. All live images were acquired with an environment chamber at 37°C. Laser lines used were 405 nm (for nuclear staining), 488 nm (for GFP-tagged proteins), 561 nm (for ATTO 590 in Cbl-fluorophore probes and Alexa 546, Alexa 594 and Alexa 568 in FISH probes and secondary antibodies) and 638 nm (for Cy5).

For live imaging of U2-OS cells, the pinhole was 1 AU, the laser power for the 488 nm line was 0.8 (40 V gain), and the laser power for the 638 nm line was 10-12 (100 V gain). The laser power for the 561 nm line was 1-1.7 (60-100 V gain) where the pinhole was 0.6-1 AU (adjusted for comparable cytosolic signal intensities between experiments). For correlative imaging to visualize the same stress granules samples live and fixed, the pinhole size was 0.6 AU. In this case, the laser power for live imaging was 1 (40 V gain) for the 488 laser line and 7 (110 V gain) for the 638 nm laser line. Fixed images for correlative imaging of stress granules were collected using a 40x Plan Apo Air objective (0.6 AU pinhole) with Nyquist sampling at 0.16 μm per pixel. The laser power for the 488 nm laser line was 2 (40 V gain) and the laser power was 1 for the 461 nm laser line (40 V gain).

For imaging of transiently produced ACTB mRNA and stress granules in fixed samples, the pinhole size was 1.1 AU, the power of the 488 nm laser line was 2 (40 V gain) and the

power of the 638 nm laser line was 1-2 (110-120 V gain), optimized for signal contrast. For imaging of endogenous ACTB mRNA, the pinhole was 1.2 AU, the laser power of the 488 nm laser line was 0.4 (40 V gain) and the laser power of the 638 nm laser line was 12 (120 V gain). The signal from the 638 nm laser line was integrated 16 times.

For live imaging of HeLa cells, the pinhole was 1.1 AU, the laser power for the 561 nm laser line was 2-5 with a gain of 50-80 V (adjusted for optimal contrast to account for differences in bead loading efficiency) and the laser power for the 488 nm laser line was 0.5 (50 V gain). For live imaging of GFP-SMN with or without co-transfection of a plasmid to produce A_T-U1 RNA, the pinhole was 1.1 AU, the laser power for the 561 nm laser line was 2 (50 V gain) and the laser power for the 488 nm laser was 0.5. The gain was adjusted for optimal signal without over-exposure of puncta in the green channel (30 V gain for the single GFP-SMN cells shown in Supplementary Fig. 18 and 50 V gain for the double transfected cell shown in Fig. 3f). For imaging of endogenous SMN and DDX20 simultaneous with U1 snRNA (either endogenous U1 snRNA or transfected to produce A_T-U1 snRNA) in fixed HeLa cells, the pinhole was 1.2 AU, the laser power for the 405 nm laser line was 2 (90 V gain), the laser power for the 561 nm laser line was 0.3 for SMN imaging and 1 for DDX20 imaging (40 V gain in all cases) and the laser power for the 638 nm laser line was 10 (120 V gain). For imaging of transiently co-transfected GFP-SMN and A_T-tagged U1 in fixed HeLa cells, the pinhole was 1.2 AU, the laser power for the 488 nm laser line was 0.3 (25 V gain) and the laser power for the 638 nm laser line was 10 (120 V gain). For imaging of coilin colocalization in fixed HeLa cells, the pinhole was 0.8, the laser power for the 405 nm laser line was 1 (100 V gain), the laser power for the 488 nm laser line was 2 (40 V gain) and the laser power for the 638 nm laser line was 4 (110 V gain).

Immunofluorescence

Cells were fixed in 4% paraformaldehyde (EM grade, Electron Microscopy Sciences) for 10 min and slides were rinse three times in PBS and permeabilized for 10 min in PBS / 0.2%

Triton X-100 at room temperature, followed by three rinses in PBS. After blocking for 30 min at room temperature in PBS / 5% FBS, slides were incubated with the primary antibody against DDX20 or SMN (both 1:200 dilution) in PBS / 5% FBS at 4°C overnight. The DDX20 antibody was a mouse monoclonal antibody (sc-57007, Santa Cruz Biotechnology) and the SMN antibody was a rabbit polyclonal antibody (sc-15320, Santa Cruz Biotechnology). After three rinses in PBS, slides were incubated with the secondary antibody (1:1,000 dilution in both cases) and Hoechst nuclear dye (1:10,000 dilution) for 90 min at room temperature. The secondary antibody for DDX20 was a goat anti-mouse Alexa 594 antibody (Invitrogen) and the secondary antibody for SMN was a donkey anti-rabbit Alexa 568 antibody (Invitrogen). Slides were rinsed three times in PBS and once in water. If no FISH was performed subsequently, slides were mounted.

Fluorescence in situ hybridization (FISH)

When no IF was performed prior to FISH, cells were fixed in 4% paraformaldehyde and permeabilized in 0.2% Triton X-100 as described above. When FISH was performed after IF, no additional permeabilization step was performed. Cells were dehydrated sequentially in 70%, 95% and 100% ethanol for 5 minutes each. After a two minute drying step, cells were rehydrated in 2x SSC (1x SSC is 150 mM NaCl, 15 mM sodium citrate dihydrate, pH 7.0) / 50% formamide (molecular biology grade) for 5 min. Slides were pre-hydrated in pre-hybridization solution for 30 min at 37°C. The pre-hybridization solution contained 50% formamide, 2x SSC, 0.5 mg/mL UltraPure Salmon sperm DNA (ThermoFisher Scientific), 1 mg/mL UltraPure BSA (ThermoFisher Scientific), 0.13 mg/mL *E. coli* tRNA (Sigma Aldrich), 1 mM Vanadyl ribonucleoside complexes solution (Signal Aldrich) and 100 mg/mL dextran sulfate in ultrapure water. After pre-hybridization, samples were hybridized with the probe in pre-hybridization solution (see Supplementary Table 5 for properties) overnight at 37°C. On the following day,

samples were washed twice in 2x SSC / 50% formamide for 30 minutes each. Slides were rinsed in PBS once and sealed.

Northern blotting

The production and processing of aptamer fusion variants was assessed in 293T cells. Prior to seeding, dishes were coated with 10 μg/mL Poly-L-Lysine for 1 h and rinsed. For each aptamer variant, ~$2x10^6$ cells were seeded in a 10 cm dish. On the following day, 15 μg plasmid DNA was transfected per 10 cm dish using the *Trans*IT (Mirus) chemical transfection system according to the manufacturer's recommendations. Cells were harvested 48 h after transfection and cell pellets were frozen at -80°C.

The total RNA was extracted using the RNeasy (Qiagen) kit according to the manufacturer's recommendation. Briefly, cell pellets were thawed on ice, resuspended in buffer RLT and lysed by passing six times through a syringe needle. The lysate was supplemented with 70% ethanol and applied to an RNeasy spin column. After on-column DNase treatment and washing steps, RNA was eluted in water. The final RNA concentration was typically 500-1000 ng/μL. The RNA was stored at -80°C for no longer than one week before proceeding.

All solutions for gel electrophoresis and Northern blotting were made in diethylpyrocarbonate (DEPC)-treated and autoclaved water to ensure removal of RNase. For each blot, RNA samples were normalized for total RNA amount (10 μg total RNA per lane). Samples with the desired amount of total RNA were tried in a SpeedVac and the RNA was brought up in 15 μL of RNA sample buffer (50% v/v formamide, 6.3% v/v formaldehyde, 0.2M MOPS, 50 mM sodium acetate pH 5.2, 10 mM EDTA pH 8.0) plus 2 μL of RNA loading buffer (50% glycerol, 1 mM EDTA pH 8.0, 0.4% Bromophenol blue, 1 mg/mL ethidium bromide). The samples were heated at 65°C for 5 min and then loaded on a 1% agarose/formaldehyde gel (50 mM sodium acetate pH 5.2, 10 mM EDTA pH 8.0, 1% w/v agarose, 6.3% formaldehyde). 10 μL

of a Low Range ssRNA Ladder (New England Biolabs) was loaded as well. The gel was run in running buffer (50 mM sodium acetate pH 5.2, 10 mM EDTA pH 8.0, 6.3% formaldehyde) at 60 V for 2.5 h. To assess the quality of the isolated RNA, the gel was then stained with ethidium bromide (10 μL of 10 mg/mL ethidium bromide in 400 mL running buffer).

After destaining in water for 5 min, the RNA was transferred to a nylon membrane as follows. Immersed in 10X SSC, two pieces of Whatman paper were placed on a stack of blotting paper, followed by the agarose gel and the pre-wet membrane (Amersham Hybond-N^+, GE Healthcare). The membrane was covered with two pieces of pre-wet Whatman paper and the RNA was allowed to transfer to the membrane by capillary transfer overnight. The RNA was then crosslinked to the membrane by exposure to UV light, followed by a washing step in 0.1X SSC and 0.1% sodium dodecyl sulfate (SDS) at 65°C for 1 h. The membrane was prehybridized for 1 h in hybridization solution (6X SSC, 10X Denhardts solution (Life Technologies), 0.1% SDS) at 42°C. The membrane was then incubated with hybridization solution supplemented with the radioactive, labeled probe overnight at 42°C. After 3 wash steps for 5 min at room temperature in washing solution (6X SSC, 0.1% SDS) and an additional wash step at 48°C for 20 min, the membrane was tried and exposed overnight. Exposure and visualization of the ^{32}P signal was done using the Phosphor Screen and Cassette System from GE Healthcare. The membrane was stripped by repeated microwaving in 0.1X SSC, 0.1% SDS to subsequently hybridize with another probe.

Radioactive probes were produced as follows. The sequence of each probe is indicated in Table S5 and probes were purchased as DNA primers from IDT. From a 100 μM stock of this DNA primer, 2 μL were mixed with 2 μL ^{32}P-ATP, 2 μL T4 Polynucleotide Kinase (PNK) (NEB), 2 μL of 10X T4 PNK buffer (NEB) in water and incubated at 37°C for at least 1 h. The DNA was then passed over a G-25 column (GE Healthcare) according to the manufacturer's recommendations to remove unincorporated ATP.

References

1. Müller-McNicoll, M. & Neugebauer, K. M. How cells get the message: dynamic assembly and function of mRNA-protein complexes. *Nat. Rev. Genet.* **14,** 275–287 (2013).
2. Gerstberger, S., Hafner, M. & Tuschl, T. A census of human RNA-binding proteins. *Nat. Rev. Genet.* **15,** 829–845 (2014).
3. Buchan, J. R. & Parker, R. Eukaryotic Stress Granules : The Ins and Outs of Translation. *Mol. Cell* **36,** 932–941 (2009).
4. Decker, C. J. & Parker, R. P-Bodies and Stress Granules : Possible Roles in the Control of Translation and mRNA Degradation. *Cold Spring Harb. Perspect. Biol.* **4,** a012286 (2012).
5. Mollet, S. *et al.* Translationally Repressed mRNA Transiently Cycles through Stress Granules during Stress. *Mol. Biol. Cell* **19,** 4469–4479 (2008).
6. Balagopal, V. & Parker, R. Polysomes, P bodies and Stress granules: States and Fates of Eukaryotic mRNAs. *Curr. Opin. Cell Biol.* **21,** 403–408 (2009).
7. Tsalikis, J. *et al.* Intracellular bacterial pathogens trigger the formation of U small nuclear RNA bodies (U bodies) through metabolic stress induction. *J. Biol. Chem.* **290,** 20904–20918 (2015).
8. Matera, A. G. & Wang, Z. A day in the life of the spliceosome. *Nat. Rev. Mol. Cell Biol.* **15,** 108–21 (2014).
9. Wu, B., Chao, J. A. & Singer, R. H. Fluorescence fluctuation spectroscopy enables quantitative imaging of single mRNAs in living cells. *Biophys. J.* **102,** 2936–44 (2012).
10. Fusco, D. *et al.* Single mRNA molecules demonstrate probabilistic movement in living mammalian cells. *Curr. Biol.* **13,** 161–7 (2003).
11. Wu, B., Chen, J. & Singer, R. H. Background free imaging of single mRNAs in live cells using split fluorescent proteins. *Sci. Rep.* **4,** 3615 (2014).
12. Garcia, J. F. & Parker, R. MS2 coat protein bound to yeast mRNAs block 5′ to 3′ degradation and trap mRNA decay products: implications for the localization of mRNAs by MS2-MCP system. *RNA* **21,** 1393–5 (2015).
13. Nguyen, D. H., DeFina, S. C., Fink, W. H. & Dieckmann, T. Binding to an RNA aptamer changes the charge distribution and conformation of malachite green. *J. Am. Chem. Soc.* **124,** 15081–15084 (2002).
14. Babendure, J. R., Adams, S. R. & Tsien, R. Y. Aptamers Switch on Fluorescence of Triphenylmethane Dyes. *J. Am. Chem. Soc.* **125,** 14716–14717 (2003).
15. Arora, A., Sunbul, M. & Jäschke, A. Dual-colour imaging of RNAs using quencher- and fluorophore-binding aptamers. *Nucleic Acids Res.* **43,** e144 (2015).
16. Sunbul, M. & Jäschke, A. Contact-mediated quenching for RNA imaging in bacteria with a fluorophore-binding aptamer. *Angew. Chem. Int. Ed. Engl.* **52,** 13401–4 (2013).
17. Paige, J. S., Wu, K. Y. & Jaffrey, S. R. RNA mimics of green fluorescent protein. *Science* **333,** 642–6 (2011).
18. Filonov, G. S., Moon, J. D., Svensen, N. & Jaffrey, S. R. Broccoli: Rapid Selection of an

RNA Mimic of Green Fluorescent Protein by Fluorescence-Based Selection and Directed Evolution. *J. Am. Chem. Soc.* **136,** 16299–308 (2014).

19. Dolgosheina, E. V *et al.* RNA Mango Aptamer-Fluorophore: A Bright, High-Affinity Complex for RNA Labeling and Tracking. *ACS Chem. Biol.* **9,** 2412–2420 (2014).

20. Trachman, R. J. *et al.* Structural basis for high-affinity fluorophore binding and activation by RNA Mango. *Nat. Chem. Biol.* **13,** 807–813 (2017).

21. Warner, K. D. *et al.* Structural basis for activity of highly efficient RNA mimics of green fluorescent protein. *Nat. Struct. Mol. Biol.* **8,** 658–63 (2014).

22. Guo, J. U. & Bartel, D. P. RNA G-quadruplexes are globally unfolded in eukaryotic cells and depleted in bacteria. *Science* **353,** aaf5371-8 (2016).

23. Jeng, S. C. Y., Chan, H. H. Y., Booy, E. P., McKenna, S. A. & Unrau, P. J. Fluorophore ligand binding and complex stabilization of the RNA Mango and RNA Spinach aptamers. *RNA* **22,** 1884–1892 (2016).

24. Ceres, P., Trausch, J. J. & Batey, R. T. Engineering modular 'ON' RNA switches using biological components. *Nucleic Acids Res.* **41,** 10449–61 (2013).

25. Ceres, P., Garst, A. D., Marcano-Velázquez, J. G. & Batey, R. T. Modularity of select riboswitch expression platforms enables facile engineering of novel genetic regulatory devices. *ACS Synth. Biol.* **2,** 463–72 (2013).

26. Johnson, J. E., Reyes, F. E., Polaski, J. T. & Batey, R. T. B12 cofactors directly stabilize an mRNA regulatory switch. *Nature* **492,** 133–7 (2012).

27. Polaski, J. T., Holmstrom, E. D., Nesbitt, D. J. & Batey, R. T. Mechanistic Insights into Cofactor-Dependent Coupling of RNA Folding and mRNA Transcription/Translation by a Cobalamin Riboswitch. *Cell Rep.* **15,** 1100–1110 (2016).

28. Lee, M. & Grissom, C. B. Design, synthesis, and characterization of fluorescent cobalamin analogues with high quantum efficiencies. *Org. Lett.* **11,** 2499–502 (2009).

29. Smeltzer, C. C. *et al.* Synthesis and characterization of fluorescent cobalamin (CobalaFluor) derivatives for imaging. *Org. Lett.* **3,** 799–801 (2001).

30. Fedosov, S. N. *et al.* Application of a fluorescent cobalamin analogue for analysis of the binding kinetics. A study employing recombinant human transcobalamin and intrinsic factor. *FEBS J.* **273,** 4742–53 (2006).

31. Chromiński, M. & Gryko, D. 'Clickable' vitamin B12 derivative. *Chem. - A Eur. J.* **19,** 5141–8 (2013).

32. Loska, R., Janiga, A. & Gryko, D. Design and synthesis of protoporphyrin IX/vitamin B-12 molecular hybrids via CuAAC reaction. *J. Porphyrins phtalocynines* **17,** 104–117 (2013).

33. Strack, R. L., Disney, M. D. & Jaffrey, S. R. A superfolding Spinach2 reveals the dynamic nature of trinucleotide repeat-containing RNA. *Nat. Methods* **10,** 1219–24 (2013).

34. Ponchon, L. & Dardel, F. Recombinant RNA technology: the tRNA scaffold. *Nat. Methods* **4,** 571–576 (2007).

35. Morisaki, T. *et al.* Real-time quantification of single RNA translation dynamics in living cells. *Science* **6392,** 1425–1429 (2016).

36. Hayashi-Takanaka, Y. *et al.* Tracking epigenetic histone modifications in single cells

using Fab-based live endogenous modification labeling. *Nucleic Acids Res.* **39,** 6475–6488 (2011).

37. McNeil, P. L. & Warder, E. Glass beads load macromolecules into living cells. *J. Cell Sci.* **88,** 669–678 (1987).

38. Nelles, D. A. *et al.* Programmable RNA Tracking in Live Cells with CRISPR/Cas9. *Cell* **165,** 488–496 (2016).

39. Zurla, C., Lifland, A. W. & Santangelo, P. J. Characterizing mRNA interactions with RNA granules during translation initiation inhibition. *PLoS ONE* **6,** e19727 (2011).

40. Jain, S. *et al.* ATPase-Modulated Stress Granules Contain a Diverse Proteome and Substructure. *Cell* **164,** 487–498 (2016).

41. McCloskey, A., Taniguchi, I., Shinmyozu, K. & Ohno, M. hnRNP C Tetramer Measures RNA Length to Classify RNA Polymerase II Transcripts for Export. *Science* **335,** 1643–1646 (2012).

42. Ishikawa, H. *et al.* Identification of truncated forms of U1 snRNA reveals a novel RNA degradation pathway during snRNP biogenesis. *Nucleic Acids Res.* **42,** 2708–2724 (2014).

43. Hutten, S., Chachami, G., Winter, U., Melchior, F. & Lamond, a. I. A role for the Cajal-body-associated SUMO isopeptidase USPL1 in snRNA transcription mediated by RNA polymerase II. *J. Cell Sci.* **127,** 1065–1078 (2014).

44. Polaski, J. T., Webster, S. M., Johnson, J. E. & Batey, R. T. Cobalamin Riboswitches Exhibit a Broad Range of Ability to Discriminate between Methylcobalamin and Adenosylcobalamin. *J. Biol. Chem.* **292,** 11650–11658 (2017).

45. Edwards, A. L., Garst, A. D. & Batey, R. T. Determining Structures of RNA Aptamers and Riboswitches by X-Ray Crystallography. *Methods Mol. Biol.* **535,** 135–63 (2009).

46. Gilbert, S. D. & Batey, R. T. Monitoring RNA-Ligand Interactions Using Isothermal Titration Calorimetry. *Methods Mol. Biol.* **540,** 97–114 (2009).

47. Quenching of Fluorescence. in *Principles of Fluorescence Spectroscopy* (ed. Lakowicz, J. R.) 277–330 (Springer, 2006).

48. Beckley, S. a, Liu, P., Stover, M. L., Gunderson, S. I. & Rowe, D. W. Reduction of Target Gene Expression by a Modified U1 snRNA Reduction of Target Gene Expression by a Modified U1 snRNA. *Mol. Cell. Biol.* **21,** 2815–25 (2001).

49. Wheeler, J., Matheny, T., Jain, S., Abrisch, R. & Parker, R. Distinct stages in stress granule assembly and disassembly. *Elife* **5,** 1–25 (2016).

50. Shpargel, K. B. & Matera, A. G. Gemin proteins are required for efficient assembly of Sm-class ribonucleoproteins. *Proc. Natl. Acad. Sci. U.S.A.* **102,** 17372–17377 (2005).

51. Shpargel, K. B. Control of Cajal body number is mediated by the coilin C-terminus. *J. Cell Sci.* **116,** 303–312 (2003).